A field investigation into the mechanisms of pile ageing in sand

Gavin, Kenneth; Igoe, David

Important note
To cite this publication, please use the final published version (if applicable).
Please check the document version above.

A field investigation into the mechanisms of pile ageing in sand

KENNETH GAVIN* and DAVID IGOE†

The design of axially loaded piles has been an area of focus for the offshore industry in recent years. A number of studies report substantial increases in the shaft capacity of piles driven in sand, known as pile ageing. The offshore industry has been slow to implement ageing into practice because of uncertainty over the mechanisms controlling ageing and variability on the impact of ageing. This paper presents the results of tests using an instrumented pile with two separate installations considered, one where the pile was load tested 4 days after installation and the second where the load test was performed after an ageing period of 116 days. Data from the installation, ageing period, load testing and pile extraction provide further insights into the mechanisms governing the effect of time on the axial capacity of piles in sand.

KEYWORDS: footings/foundations; piles & piling; sands

INTRODUCTION

The shaft resistance of piles driven in sand exhibits time-dependent increases, termed ageing. A number of separate case histories have demonstrated strong increases in pile capacity, up to three-fold over the first 100 days following driving. Despite this, pile ageing has not yet been widely incorporated into design practice because of the combined effects of variability in the degree of ageing indicated by various case studies and uncertainties about the primary mechanisms controlling the process. In this paper the results of field tests on an instrumented open-ended steel pile driven in dense sand are reported. The test programme was designed specifically to measure the radial effective stress and load distribution during installation, ageing and load testing for a recently installed pile and one that was aged for a period of 116 days. After the ageing period the pile was extracted in order to study the effect of physio-chemical reactions during the ageing period.

Background

A number of workers have reported large gains in capacity with time from field tests performed on piles driven in sand. Tavenas & Audy (1972) found that the axial capacity of driven pre-cast concrete piles increased by approximately 70% over a 20 day period after driving. Similar trends were reported by Fellenius *et al.* (1989), York *et al.* (1994), Long *et al.* (1999), Axelsson (2000a, 2000b), Jardine *et al.* (2006), Anusic *et al.* (2018) and others, see Fig. 1. A simple expression to predict the axial capacity at a given time (Q_t) of the form shown in equation (1) is commonly adopted (see Skov & Denver, 1988).

$$Q_t = Q_0 + A\log(t/t_0) \tag{1}$$

where A is a constant and Q_0 is the capacity at a reference time t_0.

Significant variability in ageing is evident in Fig. 1 where for a given pile type, time and test site the pile capacity can vary by more than 50%. Bowman & Soga (2005) and Lim & Lehane (2014) suggest that the scatter evident in these database studies arises from one or a combination of the following reasons: comparing results of dynamic (DLTs) and static load tests (SLTs); variation in the definition of reference time; load history; difficulty in separating shaft and base resistance from instrumented compression SLTs; and combining trends from tension and compression static load tests at different ageing periods.

Potential mechanisms for pile ageing were suggested by Chow (1997) including: (*a*) mechanism 1, corrosion and physio-chemical reaction; (*b*) mechanism 2, stress relaxation; and (*c*) mechanism 3, increased constrained dilation and hence radial stresses with time.

Mechanism 1, corrosion and physio-chemical reactions that develop with time lead to roughening of the pile surface and the growth of a crust of particles adhering to the pile shaft (see Gavin *et al.*, 2013a; Lim & Lehane, 2014). Gavin *et al.* (2015) suggest corrosion is not the primary mechanism as database studies showed that ageing was observed for steel, concrete and timber piles and occurred both above and below the corrosion zone.

Mechanism 2 involves a gradual breakdown of the hoop stresses developed during pile installation. With time, creep-induced stress redistribution would cause increases in stationary radial effective stress during the set-up period. Particle rearrangement as a result of creep was measured in triaxial ageing tests performed by Bowman & Soga (2003, 2005) and Kuwano & Jardine (2002). Zhang & Wang (2014) used tactile pressure sensors to measure the stress in the soil mass around a model pile during an 80 h ageing period following installation in a pile-testing chamber. They measured significant redistribution of stress, such that the radial stress increased in areas of low initial stress and reduced significantly in areas of high stress. Modest increases of radial effective stress during ageing (equalisation) have been reported in field tests on pre-cast driven concrete piles by Ng *et al.* (1988) and Axelsson (2000a); see Fig. 2. These increases were seen to occur from very low post-installation values with stresses remaining below the pre-installation horizontal effective stress even after ageing. More significant increases were measured for jacked piles by Chow (1997) and Lim & Lehane (2015). The latter report data for piles jacked into three sand deposits in Perth, Western Australia.

At these sites radial stresses increased by between 35 and 50% over a 1 day ageing period.

Mechanism 3 involves a modification of soil structure such that sand in the shear zone exhibits increased confined dilation with time. Schmertmann (1991) notes that time effects are particularly strong for sand that has undergone recent disturbance, for example from dynamic compaction or displacement pile installation. The creep-induced particle rearrangement measured by Bowman & Soga (2003) resulted in a complex structure that resulted in increased dilation during shearing of aged samples in the triaxial apparatus.

Axelsson (2000b) reported load tests on a 235 mm square concrete pile installed to a depth of 12·8 m at Fittja Straits, Sweden that was subjected to a number of reload compression tests over a 660 day ageing period. During this period the overall pile capacity increased by 60%, although the base resistance remained relatively constant. A radial

total stress sensor near the pile toe recorded modest increases due to continued dilation of around 25% during a load test performed 8 days after installation. In a test performed 660 days after installation the sensor recorded a 100% increase due to dilation during loading.

Gavin et al. (2013a) reported large increases in radial stress during loading of an open-ended pile driven in dense Blessington sand allowed to age for 219 days. They suggested that this was the primary mechanism for significant ageing of the axial tension capacity of piles tested at this site.

In order to reduce uncertainties identified in previous database studies a series of large-scale pile test programmes were initiated at a number of well-characterised geotechnical test sites including Dunkirk, France (Jardine et al., 2006), Blessington, Ireland (Gavin et al., 2013a) and Larvik, Norway (NGI, 2014). Details of the piles tested at all sites are shown in Table 1. At each site, first-time tension load tests were performed at various periods after installation. Significant increases in pile capacity were evident in most tests, for example, the piles at Dunkirk exhibited a 220% increase in shaft capacity in tests performed between 9 and 235 days after installation; see Fig. 3(a).

To compare load tests at different sites it is necessary to determine a reference capacity. To avoid ambiguities with regard to assigning a reference time capacity, such as t_0, Gavin et al. (2015), Lehane et al. (2017) and others suggest use of a cone penetration test (CPT)-based pile design method to perform the normalisation. The pile capacities measured at Dunkirk, Larvik and Blessington are compared in Table 1 with pile capacities estimated using the IC-05 design method (Jardine et al., 2005). It is apparent that the data from the three sites are reasonably consistent and well described by the intact ageing curve (IAC) proposed by Jardine et al. (2006) to describe ageing trends at Dunkirk. However, some scatter remains, even in these relatively well-controlled tests, with a notable case being the low 30 days pile capacity measured at Blessington (Table 2).

Significant advances in the design of closed-ended piles in sand were achieved through carefully controlled, instrumented pile tests that measured the radial effective stress on a pile during installation, equalisation and load testing (Lehane, 1992; Chow, 1997). The work was synthesised in the
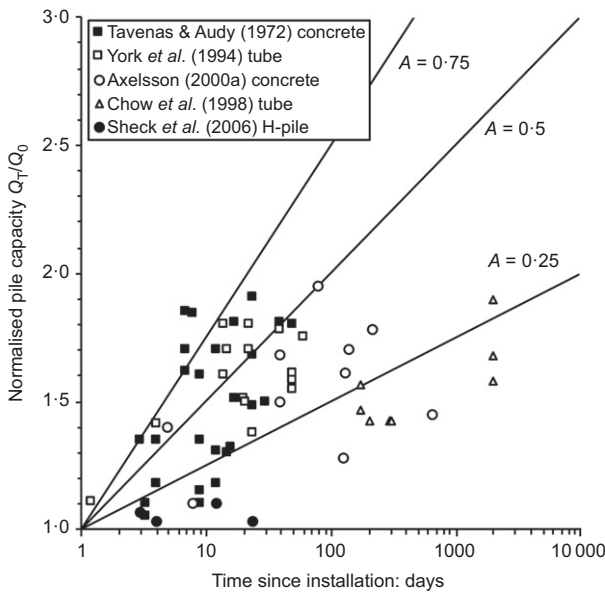

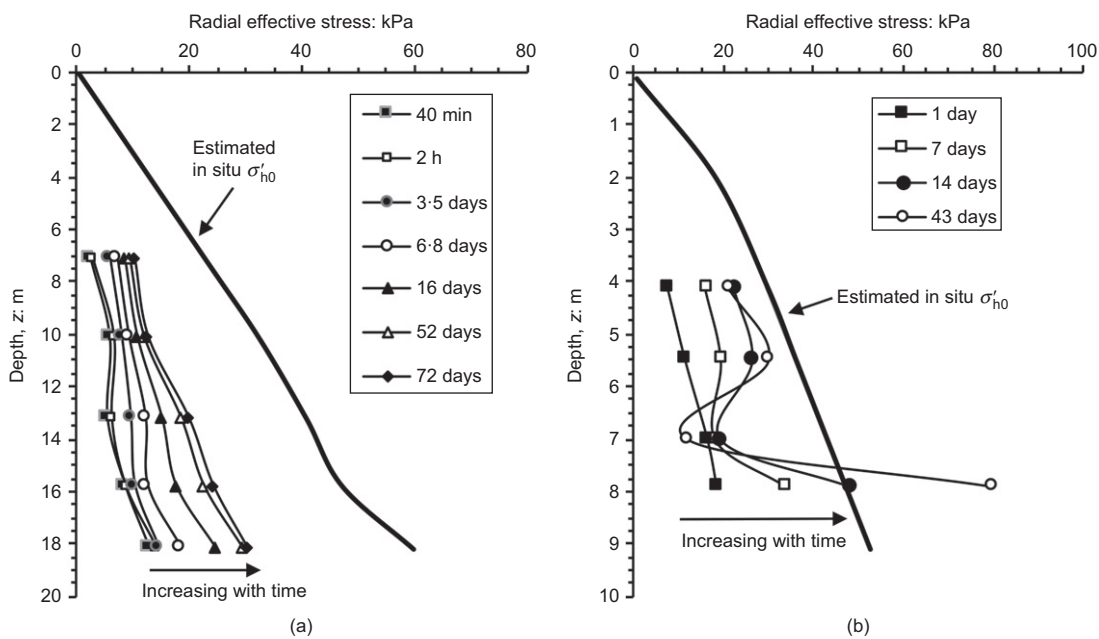Fig. 1. Case histories of pile set-up in sandy soil (after Zhang & Wang, 2014)

Fig. 2. Radial stresses measured during ageing of pre-cast driven concrete piles from (a) Hunters Point (Ng et al., 1988) and (b) Fittya Straits (Axelsson, 2000a)

Table 1. Ageing pile tests at Dunkirk

Site	Pile dimensions	Pile no.	Time: days	Pile capacity: kN	Pile capacity normalised by IC-05 prediction*
Dunkirk (Jardine *et al.*, 2006)	457 mm dia., 18·9–19·3 m long	DK1	9	1445	1·03
		DK2	81	2420	1·72
		DK3	235	3221	2·29
Karlsrud *et al.* (2014)	508 mm dia., 20·1 m long	1	42	980	2·37
		2	132	990	2·40
		3	213	1160	2·81
		4	365	1065	2·58
		5	730	1080	2·62
Gavin *et al.* (2013a)	340 mm dia., 7 m long	S2	2	344	0·82
		S3	12	665	1·55
		S4	30	385	0·90
		S5	219	990	2·22

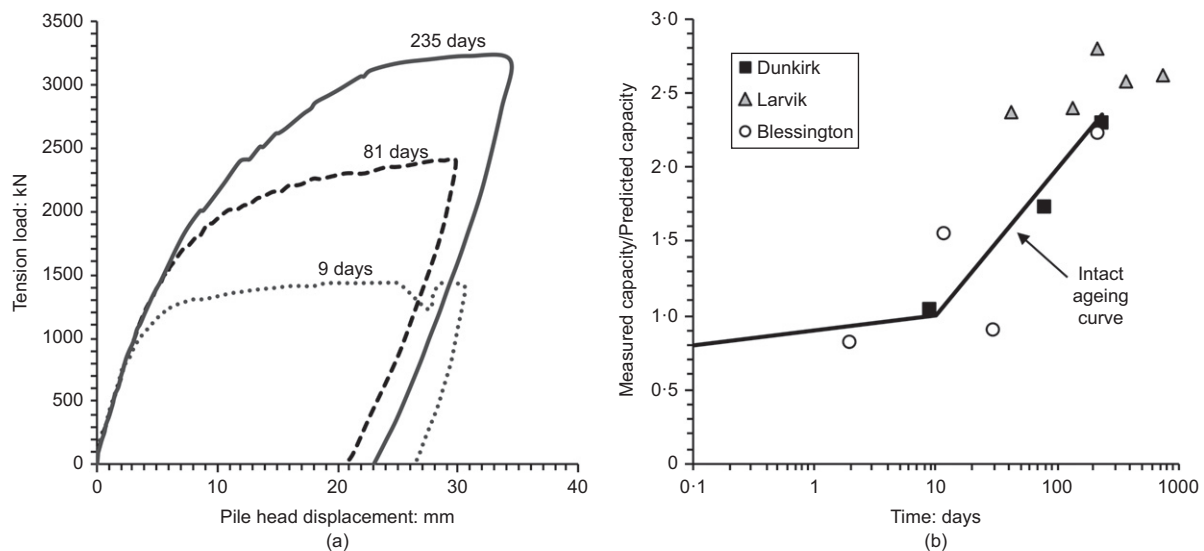*Estimates at Blessington based on local CPT profiles.

Fig. 3. (a) Ageing load test response at Dunkirk (after Jardine *et al.*, 2006). (b) Variation of normalised capacity with time

Table 2. Summary of radial stress sensor performance after installation

Instrument	Distance from toe: m	Level (h/D)	Pile S6			Pile S7		
TML PDA-PA (rated capacity of 3 MPa or 500 kPa)	0·51	1 (1·5)	A	B	C	A	B	C
	1·87	2 (5·5)	A	B	C	A	B	C
	3·57	3 (10·5)	A	B	C	A	B	C
	5·95	4 (17·5)	A	B	C	A	B	C

CPT-based design approaches ICP-05 (Jardine *et al.*, 2005) and UWA-05 (Lehane *et al.*, 2005), which have been shown to provide reliable estimates of pile shaft capacity in sand (Schneider *et al.*, 2007). In order to understand the mechanism of ageing, similar data are required, particularly for open-ended piles typically used offshore. This paper presents the results from instrumented pile tests that examined the effect of time since installation on the radial and shear stress developed on an open-ended pile, driven in dense sand.

DESCRIPTION OF FIELD TESTS

Pile tests performed on an instrumented open-ended steel pipe pile are described in this paper. The test pile had an external diameter, *D*, of 340 mm and wall thickness of 14 mm. The pile was driven to a tip level 7 m below ground level (bgl)

and load tested after a set-up period of 116 days (pile S6). Subsequently it was extracted and re-driven at a new location to a penetration depth of 6·5 m. This pile, designated S7, was load tested 4 days after installation. The site conditions and test pile details are described in this section.

Site description

The test site is an active quarry located near the village of Blessington in Ireland. The site has been used to investigate the field response of a number of foundation systems; see Gavin & O'Kelly (2007), Gavin *et al.* (2009), Igoe *et al.* (2011) and others. The soil at the location is a glacially deposited, dense fine sand with a CPT end resistance, q_c (see Fig. 4(a)), reported in Igoe & Gavin (2019) that increases from ≈10 MPa near the ground surface to 15–20 MPa over
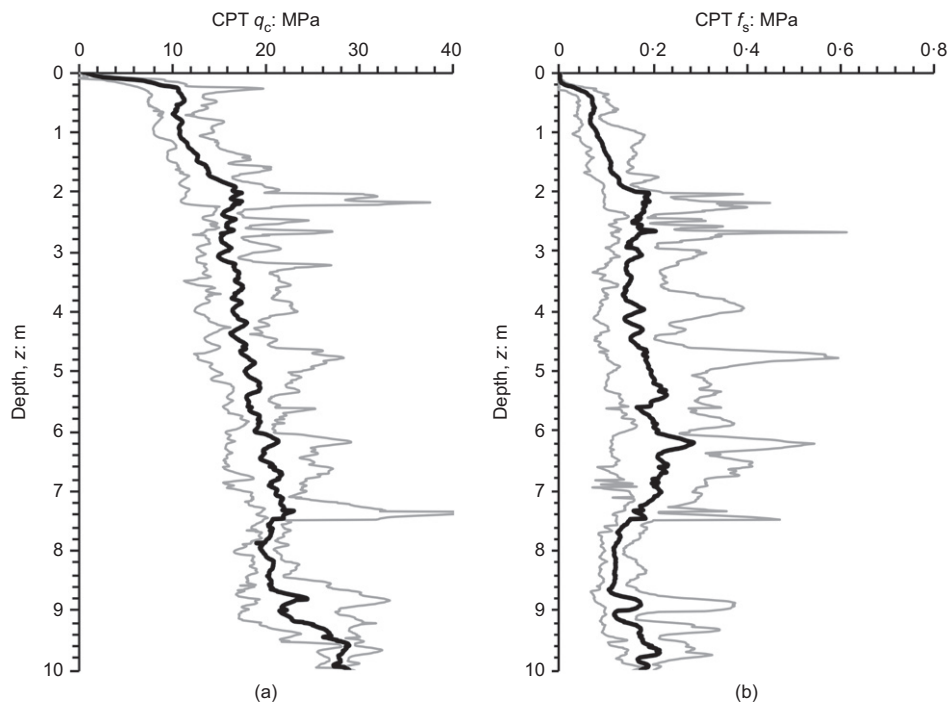
Fig. 4. (a) CPT cone resistance; (b) CPT sleeve friction at Blessington. The grey lines represent minimum and maximum values, the black lines represent the average values

the depth of penetration of the test piles. The data in Fig. 4(a) show the average (in bold) maximum and minimum values of CPT q_c measured from eight profiles taken in the vicinity of the test piles. The CPT shaft friction, f_s, values in Fig. 4(b) show slightly larger variability with an average friction ratio (f_s/q_c) of 1%.

The water table is approximately 13 m bgl with the result that the sand in which the test pile was embedded is partially saturated. The moisture content of the deposit increases from 8% at ground surface to approximately 12% at 4·5 m depth. The in situ suctions measured used piezometers pushed into pre-drilled auger holes indicate values of between 5 and

10 kPa, which are negligible when compared to horizontal effective stresses developed by test piles in this deposit. Laboratory testing was used to supplement the in situ site investigation and establish basic soil properties. Particle size analyses classified the material as fine grained, with a median particle size varying from 0·1 to 0·15 mm. Dilatometer testing (DMT) performed at 250 mm depth intervals indicated lift-off and limit pressures that increased rapidly with depth, with lift-off pressure in the range of 500–1000 kPa and limit pressures in the range of 2000–3000 kPa over the penetration depth of the test pile (Fig. 5(a)). Profiles of the estimated coefficient of earth pressure at rest, K_0, based
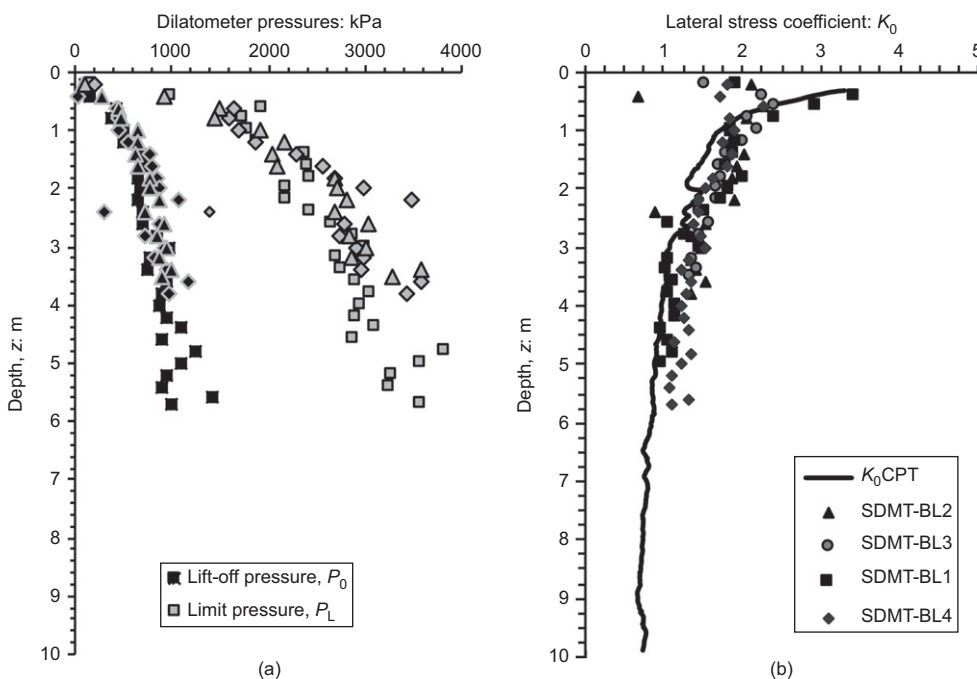

Fig. 5. (a) Dilatometer lift and limit pressures and (b) estimated coefficient of earth pressure at rest, K_0 values for Blessington

on correlations with the CPT and DMT tests, are in good agreement and are shown in Fig. 5(b). Detailed descriptions of the geotechnical properties of Blessington Sand are given in Tolooiyan & Gavin (2013) and Igoe & Gavin (2019).

Pile instrumentation

The test pile was instrumented with 12 miniature total stress sensors, 20 strain gauges and ten temperature sensors. The layout of the instrumentation is shown in Fig. 6. Three miniature total stress sensors, type pressure sensor reference number TML PDA-PA, were installed at each of four levels (1·5, 5·5, 10·5 and 17·5 diameters from the pile toe). Mechanical protection for the sensor lead wires was provided by two channels, which were welded onto the pile outer wall. Each channel was fabricated from two 16×16 mm steel strips, which formed the channel walls, covered over with a 40×3 mm steel strip. The channels were placed diametrically opposite each other and ran the length of the pile, stopping 500 mm from the top of the pile to allow the cables to exit. The strain gauges and temperature sensors were housed inside the channels, while the miniature total stress sensors were housed outside the channels and circumferentially offset by $\sim 90°$ to minimise disturbance caused by the change in geometry due to the channels.

The total stress sensors were placed in pre-drilled slots with the cable exiting through a recessed channel in the pile wall (backfilled with epoxy resin for mechanical protection), which ran into the main steel channels. At the top of the pile the lead wires were soldered to a shielded multi-core cable, which was clamped in place. All solders were made using heat-shrink solder sleeves to ensure an adequate insulation and protection from moisture ingress. During handling and installation some of the sensors were damaged and unusable for the duration of testing. The decision to provide three miniature total stress sensors at each level (designated A, B and C; see Table 1) was based on experience from installing a previous instrumented test pile at the site (see Gavin *et al.*, 2013a, 2013b) where sensor damage during installation occurred. During the first

installation, test S6, three sensors were damaged (one near the pile toe, sensor B) and two near the pile head (sensors A and B). During reinstallation of the pile (S7) an additional three sensors were damaged (at h/D levels of 5·5 and 10). Because of the importance of measuring stress near the pile toe, the installation of the pile was stopped at a depth of 6·5 m bgl to prevent further instrument damage and to ensure at least two operational sensors remained at the most important locations. Another limitation of these sensors that should be considered is the potential for shielding of stresses in the sand mass if material adheres to the pile shaft. All strain gauges and temperature sensors remained fully operational throughout the test programme.

TEST RESULTS

This section describes the pile performance during the installation, equalisation and load test phases.

Pile installation

The blow-counts required to drive the piles are shown in Fig. 7(a). Both piles S6 and S7 were driven using a PM20 Junttan piling rig with a 5 t HHK-5A hammer. For pile S6, a stroke length of 0·2 m was used for the first 4 m of installation; this was gradually increased to 0·35 m over the last 3 m of driving until the final penetration depth of 7 m was reached. For pile S7 the hammer stroke was varied from 0·2 to 0·5 m. The maximum energy (EMX) transferred into pile S7 was measured during pile driving using accelerometers and strain gauges attached to the pile along with a pile-driving analyser (PDA). The EMX transferred into pile S6 was estimated based on the hammer properties and drop height. Flynn & McCabe (2016) used EMX measurements with the same piling hammer from multiple sites to determine the ratio of EMX to rated hammer energy as a function of drop height, showing a strong linear correlation. Using a best-fit linear trend line through the data, the following equation was used to estimate the EMX for pile S6

$$\text{EMX} = \left(\frac{100 - \Delta E_{\text{cushion}}}{100} \right) \times (-0.06 + 112.86 h_{\text{avg}}) \times E_{\text{rated}}$$

(2)

where $\Delta E_{\text{cushion}}$ is the percentage energy loss due to the piling cushion (assumed to be 20%) and h_{avg} is the average hammer drop height and E_{rated} is the rated energy of the hammer (59 kNm). A comparison of the energy from both piles is provided in Fig. 7(c) and explains the significantly higher blow counts from S6 compared with S7. Despite the different blow counts noted during installation, both piles provide a very good match with the ageing pile capacity trend from identical piles installed at the site (S2–S5; Gavin *et al.*, 2013a, 2013b) indicating that the end of driving capacity was not significantly affected by the blow counts.

Driving was paused at intervals of 0·25 m to record the stationary radial stress and soil plug length. The incremental filling ratio (IFR) (the change in plug length per increment of pile penetration) is shown in Fig. 7(b) for pile S6. The pile was almost fully coring (IFR > 85%) for the first 2 m of penetration. Below this depth IFR reduces with depth with a final IFR value at 7 m of 40%. Unfortunately, the plumb line used to measure the IFR profile for pile S7 was damaged at the start of installation and therefore it was not possible to record the IFR for pile S7.

The stationary radial stresses measured in pause periods during the installation of pile S6 are shown in Fig. 8. Since the sand is partially saturated and previous model pile tests indicated no pore pressure build-up during installation, the
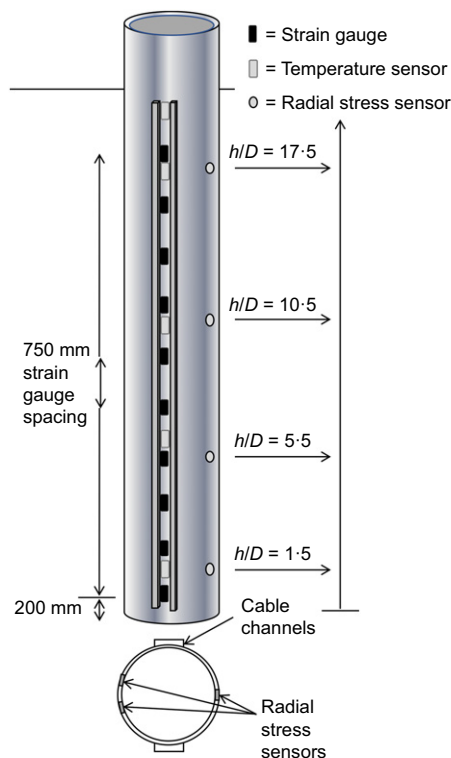

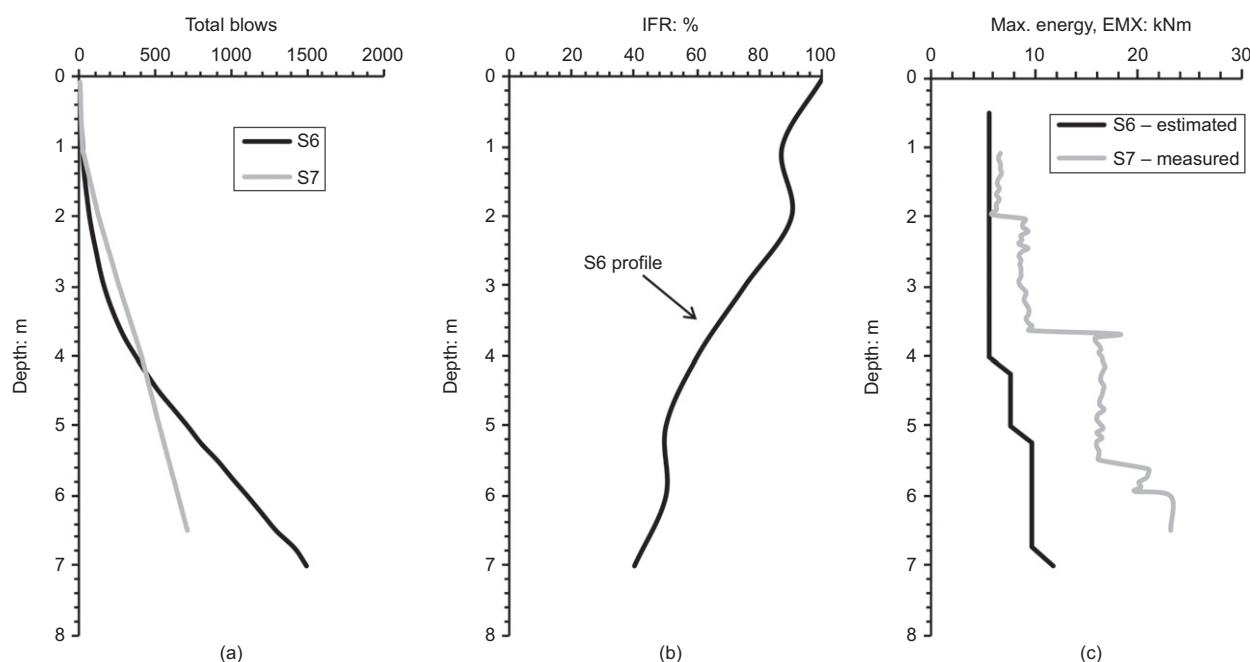**Fig. 6. Layout of pile instrumentation**

Fig. 7. (a) Total blows; (b) incremental filling ratio during pile installation; (c) energy measurements during pile installation
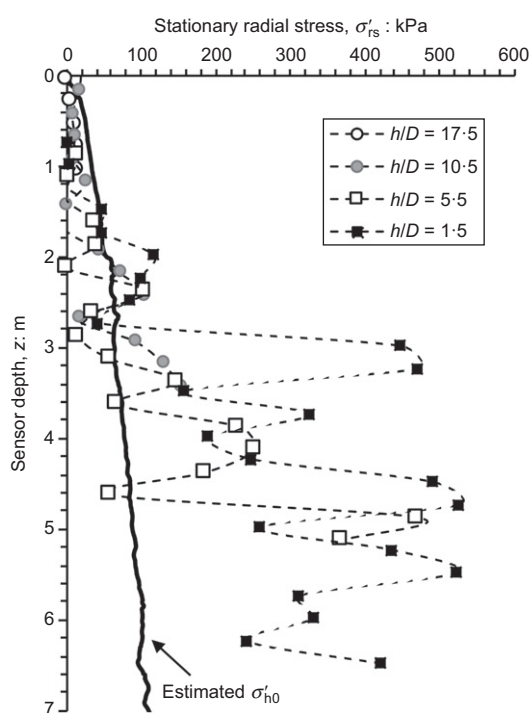

Fig. 8. Stationary radial stresses measured during driving pause periods for pile S6

sensors was consistent for both the tests described in this paper and in agreement with the trends noted in Gavin *et al.* (2013a). During pile installation to 3 m bgl, the radial stress values at all h/D levels, were scattered around the estimated in situ horizontal stress, σ'_{h0}. During driving, when the sensors were located at depths in excess of 3 m, the depth coinciding with onset of plugging (see Fig. 7(c)), the radial stresses increased significantly, being 2 to 6 times higher than σ'_{h0}, with the higher ratios measured at the sensors closest to the pile tip ($h/D = 1.5$ and 5.5).

The strain gauges allowed the residual load that developed during installation to be estimated. At the end of installation of pile S6, a significant residual load existed, see Fig. 9. The peak load measured near the pile tip was 364 kN, which corresponds to a base pressure of ≈ 4.2 MPa or $\approx 20\%$ of the q_c value at the pile tip. Gavin & Lehane (2007) report base residual stresses of between 2.4 MPa and 7.3 MPa developed by a jacked, open-ended pile at the test site, with the residual stress increasing as IFR reduced. Interestingly for pile S6 the residual load at all levels on the pile dropped in the 40 min monitoring period following the end of driving, with the value near the pile tip reducing by 40%, see Fig. 9. Given that elastic decompression of the pile would occur almost instantaneously following the last hammer blow, the reduction of the residual load in this period must have been associated with relaxation in the soil mass.

Ageing period
Following installation, a battery-powered Campbell Scientific cr800 data-logger was used to provide measurements of the radial stress every 30 min for the duration of the ageing period on the test piles. The values measured on both piles were comparable and data from the pile S6 with the longer ageing period are shown in Fig. 10. The following trends are noteworthy.

(*a*) Immediately after installation the radial stresses were highest near the pile tip ($h/D = 1.5$ and 5.5).
(*b*) The radial stress at all h/D levels reduced over time, with the largest reductions occurring nearest the pile tip

stationary radial stresses are assumed to be equivalent to the short-term radial effective stresses (σ'_{rs}). It is evident that, for a given sensor depth, a relatively wide variation of σ'_{rs} was measured; for example, the sensor at $h/D = 1.5$ recorded σ'_{rs} values in the range 188–560 kPa at depths between 3 m and 6 m. Part of this variability may be due to instrument zero shifts, the small sensing face and soil smear, or they could reflect geological variability. For these reasons it is difficult to verify the absolute values of the sensor readings (laboratory calibration of these sensors is extremely difficult because of the complex boundary conditions involved, see Zhu *et al.* (2009) and Kirwan (2015)). Nonetheless, the general response of the
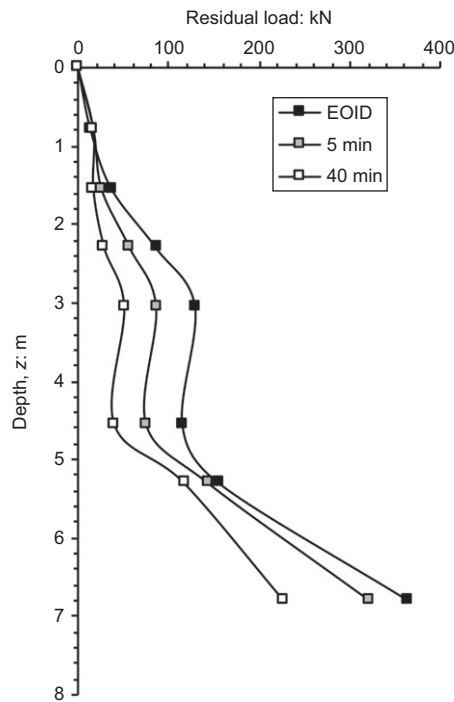
Fig. 9. Residual loads measured on pile S6 using strain gauges. EOID, end of installation
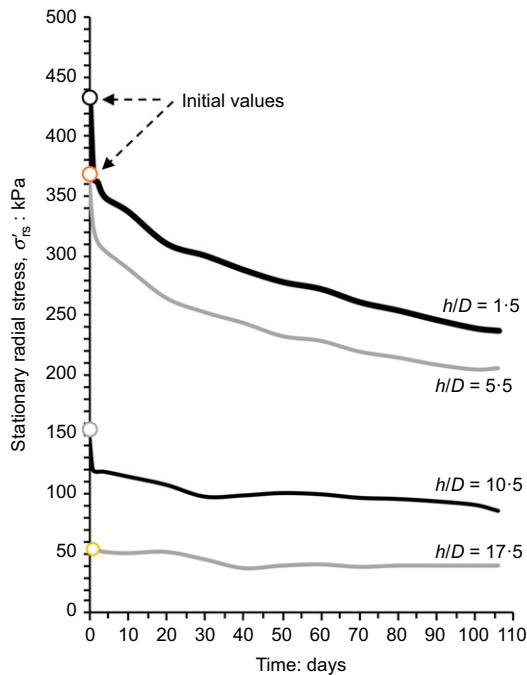

Fig. 10. Changes in radial stress during ageing of pile S6

(at $h/D = 1{\cdot}5$ and $5{\cdot}5$). Notable reductions in radial stresses occurred in the hours immediately following pile driving, with reductions of 10 to 15% of the peak values measured at $h/D = 1{\cdot}5$ and $5{\cdot}5$ over the first 24 h.

(c) These reductions in radial stresses continued over the entire ageing period, although they appeared to be reaching asymptotic values (at least for sensors remote from the pile base) after $\sim$100 days. This tendency for radial stress to reduce with time is in agreement with previous measurements from pile S5 at the same site (Gavin et al., 2013a, 2013b). However, it contrasts with

the data shown in Fig. 2, which increased with time; but at all sites there is a tendency for the measured stress to approach the in situ horizontal stress before pile installation, suggesting recovery of installation damage as hypothesised by Lim & Lehane (2014).

The data are recast in Fig. 11, in which profiles of the radial effective stress profile with depth at various times (0 to 100 days) during the ageing period are compared to the σ'_{rc} profiles predicted using the IC-05 and UWA-05 CPT methods for open-ended piles. Also shown in Fig. 11(b) are data from Gavin et al. (2013a, 2013b) measured during a 220 day ageing period on pile S5. It is evident that although the design methods underestimate the installation stress, given they are calibrated to predict the medium-term (10–30 day) stress, they provide reasonable estimates for the appropriate time period. It is evident that for the sensors remote from the pile tip ($h/D = 10{\cdot}5$ and $17{\cdot}5$), the horizontal stress measured at the pile–soil interface reduces to long-term values which are very close to the estimated in situ σ'_{h0}. For the two sensor levels nearest the pile tip, the effect of plugging during installation (below 3 m) and the presence of large residual loads in the vicinity of the pile base, result in radial stresses that remain significantly higher than σ'_{h0}.

It is clear that the effects of installation, particularly the plugging effect, led to large increases in vertical and horizontal stresses around the test piles. For the dense Blessington sand, these stresses were considerably higher than the pre-installation in situ stress and, following installation, much lower far-field σ'_{h0} and σ'_{v0} values existed. From the strain gauges' data (residual load) and radial stress sensors, it appears that stress redistribution leads to reductions in radial stress near the pile shaft and vertical stress at the pile base.

Load testing

The load–displacement response of piles S6 and S7 during maintained load static tension tests performed 116 days and 4 days after driving, respectively, are shown in Fig. 12. The tests were performed using a fully automated load-controlled hydraulic system. The test procedure involved 40 kN load steps, with the load maintained for 5 min at each increment. The data are compared to load tests performed on the same site on identical 7 m long piles S2 to S5 reported by Gavin et al. (2013a, 2013b) (data shown by dotted lines).

The pile capacity increased significantly with time from 340 kN at 1 day after installation to approximately 1000 kN after 116 days. The 1 day tension capacity is comparable to the residual load developed at the end of installation, see Fig. 9. The capacity of piles tested 116 and 219 days after installation were very similar, suggesting that the pile developed its maximum resistance during the first 5 months. As pile S7 had a slightly smaller penetration length to allow direct comparison, the average shaft resistance (q_{sav}) developed during pile loading is plotted in Fig. 12(b). This shows that q_{sav} increased from 45 kPa to a peak of 140 kPa owing to the ageing period; however, the initial pile stiffness up to q_{sav} of 25 kPa did not vary with time.

For the two piles tested in the current series, during testing of pile S6 large creep displacements were noted when the load exceeded 1020 kN at a displacement of $\approx 3{\cdot}5\%$ of the pile diameter (≈ 12 mm). For pile S7 significant creep occurred at a pile head load of 400 kN and the pile reached failure as defined by a displacement of 10% of the pile diameter during this loading step, with the load increasing as the pile moved downward.

Measurements of the radial stresses during the load tests are shown in Fig. 13. The radial stress response of pile S6 is broadly comparable to measurements from the aged pile S5
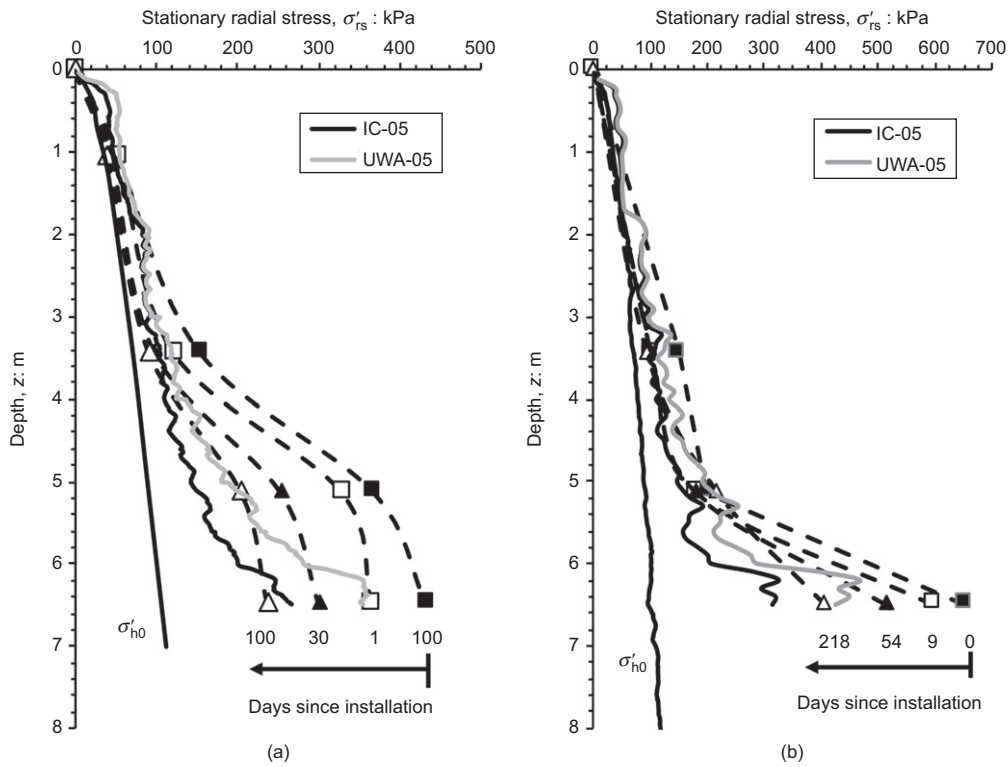
Fig. 11. Radial stress profiles measured over ageing period: (a) from pile S6; (b) from pile S5
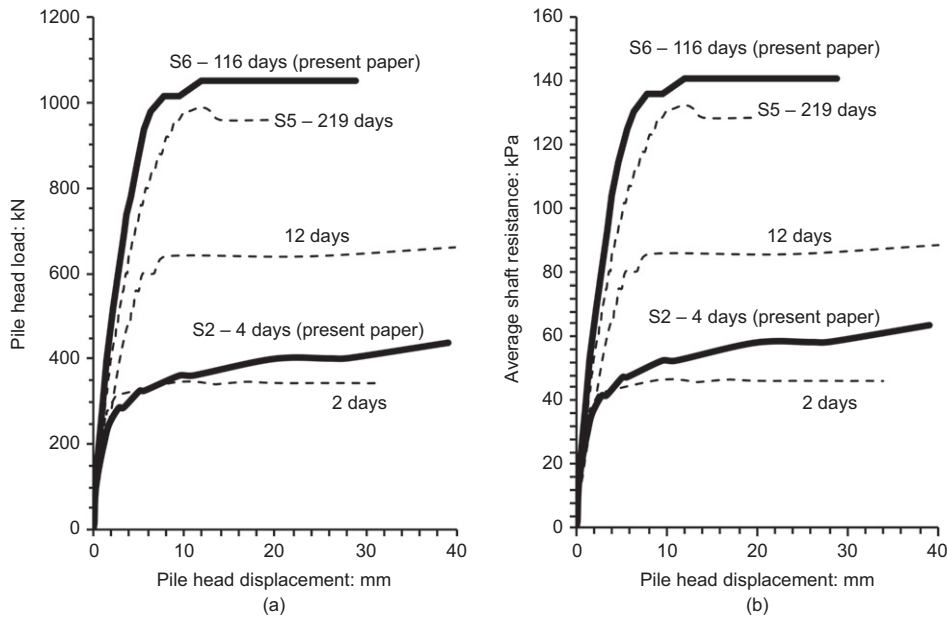

Fig. 12. (a) Pile head load–displacement response for piles S6 and S7 compared with those in Gavin *et al.* (2013a, 2013b) and (b) average shaft resistance

reported by Gavin *et al.* (2013a, 2013b). The following points are noted.

(a) For pile S6, which was allowed to age for 116 days, Fig. 13, all sensors show slight reductions in the radial stress at the start of the load test. The sensors closest to the pile tip ($h/D = 1.5$ and 5.5) then measured significant increases in radial stress $\sim$240 kPa and $\sim$150 kPa at $h/D = 1.5$ and 5.5, respectively, as the pile displacement increased. The small reduction at the start of loading is most likely due to the change in loading

direction from compression during installation to tension in the load test. See Lehane (1992) and Chow (1997).

(b) At the upper sensor levels ($h/D = 10.5$ and 17.5), stress reductions occurred throughout the load test.

(c) For pile S7, load tested 4 days after installation, the radial stresses at the bottom of the pile ($h/D = 1.5$) increased initially by $\sim$20–30 kPa, before reducing to lower than pre-test values at higher load levels.

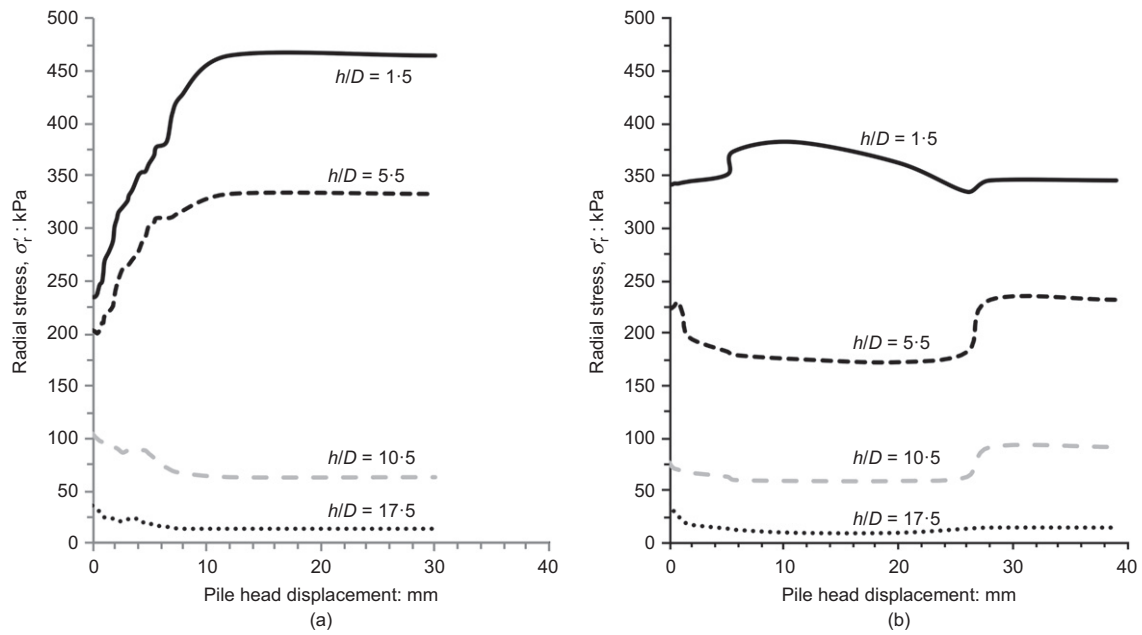(d) At all other sensor levels on pile S7, the radial stresses reduce initially before increasing at the higher load

Fig. 13. Radial stress during load test on (a) pile S6 at 116 days and (b) pile S7 at 4 days

levels; however, at the peak load the values are similar to pre-test values.

The strain gauges placed at multiple levels along the shaft of piles S6 and S7 allowed the distribution of load and shear stresses along the pile to be determined; see Fig. 14. The self-weight of the internal soil plug was estimated to contribute less than 1% (<10 kN) to the tension capacity and was thus ignored in the shear stress calculation. It is apparent from the data, see Fig. 4, that the load transfer and shear stress mobilised between ground level and 3 m bgl. was relatively low. The majority of the resistance developed by both piles was in the region from 3 m to 7 m bgl, with shear stresses being much higher near the pile tip. During the ageing period the shear stress in the region between 3 m and 7 m bgl increased significantly, whereas those closer to ground level did not appear to change. For comparative

purposes the radial stresses measured at the peak load were converted to shear stresses (assuming Mohr–Coulomb behaviour with an interface friction angle of 29°) and are shown as squares in Fig. 14(b). The back-calculated values are in good agreement with the measured data, providing confidence in the reliability of the radial stress measurements and suggesting that the shear resistance is fully mobilised during the load test.

Pile extraction and observation
After the load tests were completed the sand around the pile was carefully excavated and the pile was removed from the ground. In keeping with observations from Chow *et al.* (1998), Lehane *et al.* (2012) and others a cemented crust of sand was found to be adhered to the side of the aged piles, S5
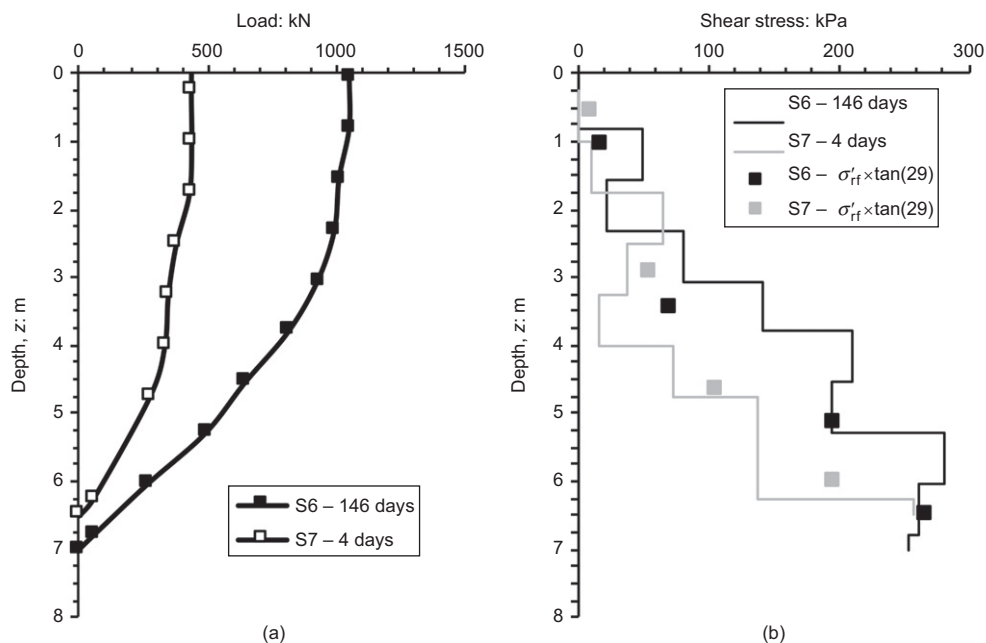

Fig. 14. Comparison of (a) load measured and (b) distribution of shear stress on piles S6 and S7
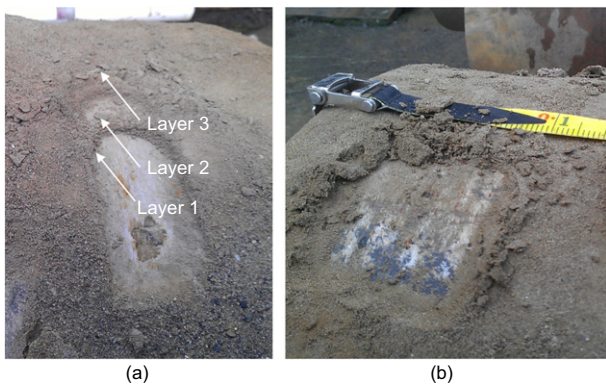
Fig. 15. Photographs of cemented sand crust adhered to pile S6 following extraction: (a) cemented sand crust on pile with distinct layers; (b) difficulty removing layer 1

(Gavin *et al.*, 2013a) and S6, over the lower 4 to 5 m of the pile shaft; see Fig. 15(a). Yang *et al.* (2010) describe three distinct layers that formed on their model piles and a similar structure developed on pile S6. The first layer – see Fig. 15(b) – was cemented to the pile shaft and was very difficult to remove. The second and third layers were attached to the first layer and remained adhered to the pile when extracted from the ground, but could be removed with moderate effort. The second and third layers were comparable to zones 1 and 2 described by Yang *et al.* (2010), while the first layer was deemed to have been originally a zone 1 material which had become bonded to the steel shaft through physiochemical processes.

Energy-dispersive X-ray spectrometry (EDS) was conducted on samples taken from the different layers and soil samples taken that had been recovered from a sonic coring borehole located adjacent to the areas in which the piles were installed. The purpose was to investigate whether any changes in the chemical composition of the sand had occurred during the ageing period. The EDS spectra from all samples revealed predominantly quartz with some calcite and occasional hints of kaolinite. In the borehole samples very little calcium was seen in the sample spectra. However, calcium was detected in nearly all the samples recovered from the pile. Some spectra from the cemented layer showed almost equal amounts of quartz and calcium with large amounts of iron present also, indicating that chemical bonding occurred with the steel pile. The authors suggest the increased calcium in samples taken from the pile shaft could relate to chemical bonding between the sand and calcium bicarbonates precipitating out of the pore water, as suggested by Kirwan (2015). Although the number of EDS spectra from each sample was too small for any meaningful statistical analysis, there was a very marked difference in the spectra of samples taken from the borehole compared to those from the pile shaft.

In addition to the EDS analysis, the roundness and sphericity of the samples taken from the pile shaft and borehole samples were determined using scanning electron microscopy (SEM) and J-image software for image processing. The roundness, R, was determined as follows

$$R = \frac{4A_c}{\pi L_{major}^2} \tag{3}$$

where A_c is the cross-sectional area of the particle and L_{major} is the length of the major axis. The sphericity, S, was determined as the ratio of the largest inscribed circle to the radius of the circumscribed circle centred at the particles' centre of mass. From the borehole samples taken, very little variation was noted with depth with average roundness values of 0·595 and sphericity values of 0·503. For samples

taken from the layer 1 and 2 material from the pile shaft, a slight increase (of approximately 10%) in roundness and sphericity was noted, with average values of 0·638 and 0·556, respectively. Such slight differences would not be significant enough to cause any notable difference in the mechanical behaviour of the sand. These findings are generally in agreement with the laboratory measurements of zone 1 and 2 material described by Yang *et al.* (2010).

The presence of an adhered crust of sand on the aged piles would lead to migration of the shear failure plane from the pile–soil interface to the sand mass. The increase in the operational friction angle from 29° (pile–soil), see Doherty *et al.* (2012) to the constant volume friction angle of $\phi'_{cv} = 36°$ would lead to an increase in mobilised shear stress of approximately 30%. It is worth noting that it is possible that the growth of the crust could lead to the radial stress sensors on the pile wall being somewhat shielded from the radial stress gradient away from the pile, and may also partly explain the reductions in radial stress measured.

CONCLUSIONS

Radial stress and load distributions measured from two instrumented open-ended driven pile tests drive in dense sand revealed the following.

(*a*) Large radial stresses were generated during pile installation that were significantly higher than the in situ horizontal stress. Continuous measurements of the radial stress measured after installation show the radial stresses (particularly near the pile toe) reduce over time but remain above the in situ horizontal stress. The radial stresses after 30+ days were comparable to predicted radial stresses from recent CPT-based design methods. The reduction in radial stress over time, with one hypothesis that ageing is caused by breakdown of the circumferential stress, can lead to an increase radial stress over time. It is possible, however, that the growth of a cemented crust on the pile surface may have shielded the sensors from the radial stress gradients away from the pile.

(*b*) During tension static load testing, very large increases in radial stress due to dilation were noted for piles which had been allowed to age for more than 100 days. A static tension test on a comparable pile 4 days after driving shows slight reductions in the radial stresses during loading, indicating that increased confined dilation was the primary mechanism for pile ageing at Blessington.

(*c*) After load testing, the aged piles were extracted from the ground and examined. A notable crust was adhered to the pile shaft for piles left in the ground for several months, which could be defined as three distinct layers. EDS spectra from samples taken from each layer indicated that physiochemical processes, possibly involving groundwater, caused some chemical bonding of the sand particles to the pile shaft.

Based on the findings of these experiments and previous work by other researchers, the authors suggest that the tendency for the tension resistance of a pile driven in sand to increase with time is due to a combination of time-dependent processes involving stress redistribution, particle rearrangement and physiochemical processes.

following industry partners for their on-going support: Mainstream Renewable Power, Bullivant Taranto and Lloyds Acoustics. The authors would like further to thank the following colleagues and technical staff at University College Dublin who provided invaluable help during the instrumentation of the piles and field tests: Lisa Kirwan, Paul Doherty, Tim Hennessy, Weichao Lee and Frank Dillon.

NOTATION

A	ageing factor
A_c	cross-sectional area of particle
D	external pile diameter (m)
E_{rated}	rated energy of piling hammer
F_s	cone penetration test (CPT) sleeve friction
h	distance from pile toe (m)
h_{avg}	average hammer drop height
K_0	coefficient of earth pressure at rest
L_{major}	length of the particle's major axis
P_L	dilatometer limit pressure
P_0	dilatometer lift-off pressure
p_{ref}	reference pressure (kPa)
Q_t, Q_0	pile capacity at time t and t_0, respectively
q_c	CPT cone resistance (MPa)
q_{sav}	average shaft resistance
R	pile outer radius (m)
t	time
t_0	a reference time
$\Delta E_{cushion}$	percentage energy loss due to the piling cushion
δ_f	interface friction angle at failure (degrees)
σ'_{h0}	horizontal effective stress prior to pile installation (kPa)
σ'_{rs}	stationary radial effective stress on a pile (kPa)
τ_f	shaft friction at failure (kPa)
ϕ'_{cv}	constant-volume friction angle

REFERENCES

Anusic, I., Lehane, B., Eiksund, G. R. & Liingaard, M. A. (2018). Evauation of installation effects on the set-up of field displacement piles in sand. *Can. Geotech. J.* **56**, No. 4, 461–472.

Axelsson, G. (2000a). *Long term set-up of driven piles in sand*. PhD thesis, Department of Civil and Environmental Engineering, Royal Institute of Technology, Stockholm, Sweden.

Axelsson, G. (2000b). Effect of constrained dilatancy during loading. *Proceedings of the international conference on geotechnical and geotechnical engineering, GeoEng 2000*, Melbourne, Australia.

Bowman, E. T. & Soga, K. (2003). Creep, ageing and microstructural change in dense granular materials. *Soils Found.* **43**, No. 4, 107–117.

Bowman, E. T. & Soga, K. (2005). Mechanisms of setup of displacement piles in sand: laboratory creep tests. *Can. Geotech. J.* **42**, No. 5, 1391–1407.

Chow, F. (1997). *Investigations into behaviour of displacement piles for offshore structures*. PhD thesis, University of London, Imperial College, London, UK.

Chow, F. C., Jardine, R. J., Brucy, F. & Nauroy, J. F. (1998). Effects of time on capacity of pipe piles in dense marine sand. *J. Geotech. Geoenviron. Engng* **124**, No. 3, 254–264.

Doherty, P., Kirwan, L., Gavin, K., Igoe, D., Tyrrell, S., Ward, D. & O'Kelly, B. (2012). Soil properties at the UCD geotechnical research site at Blessington. *Proceedings of the bridge and concrete research in Ireland conference*, Dublin, Ireland.

Fellenius, B. H., Riker, R. E., O'Brein, A. J. & Tracy, G. R. (1989). Dynamic and static testing in soil exhibiting set-up. *J. Geotech. Engng* **115**, No. 7, 984–1001.

Flynn, K. & McCabe, B. (2016). Energy transfer ratio for hydraulic pile driving hammers. *Proceedings of the civil engineering research in Ireland (CERI) conference*, Galway, Ireland, https://doi.org/10.13025/S8V881.

Gavin, K. G. & Lehane, B. M. (2007). Base load–displacement response of piles in sand. *Can. Geotech. J.* **44**, No. 9, 1053–1063.

Gavin, K. G. & O'Kelly, B. C. (2007). Effect of friction fatigue on pile capacity in dense sand. *J. Geotech. Geoenviron. Engng* **133**, No. 1, 63–71.

Gavin, K. G., Adekunte, A. & O'Kelly, B. (2009). A field investigation of vertical footing response on sand. *Proc. Instn Civ. Engrs – Geotech. Engng* **162**, No. 5, 257–267, https://doi.org/10.1680/geng.2009.I62.5.257.

Gavin, K., Igoe, D. & Kirwan, L. (2013a). The effect of ageing on the axial capacity of piles in sand. *Proc. Instn Civ. Engrs – Geotech. Engng* **166**, No. 2, 122–130, https://doi.org/10.1680/geng.12.00064.

Gavin, K., Cadogan, D., Tolooiyan, A. & Casey, P. (2013b). The base resistance of non-displacement piles in sand: part I. *Proc. Instn Civ. Engrs – Geotech. Engng* **166**, No. 6, 540–548, https://doi.org/10.1680/geng.11.00100.

Gavin, K., Jardine, R. J., Karlsrud, K. & Lehane, B. M. (2015). The effects of pile ageing on the shaft capacity of offshore piles in sand. In *Frontiers in offshore geotechnics III* (ed. V. Meyer), vol. 1, pp. 129–151. London, UK: Taylor & Francis Group.

Igoe, D. & Gavin, K. (2019). Characterization of the Blessington sand geotechnical test site. *Aims Geosci.* **5**, No. 2, 145–162.

Igoe, D., Gavin, K. G. & O'Kelly, B. (2011). The shaft capacity of pipe piles in sand. *ASCE J. Geotech. Geoenviron. Engng* **137**, No. 10, 903–912, https://doi.org/10.1061/(ASCE)GT.1943.5606.0000511.

Jardine, R., Chow, F., Overy, R. & Standing, J. (2005). *ICP design methods for driven piles in sands and clays*. London, UK: Thomas Telford.

Jardine, R., Standing, J. & Chow, F. (2006). Some observations of the effects of time on the capacity of piles driven in sand. *Géotechnique* **55**, No. 4, 227–244, https://doi.org/10.1680/geot.2006.56.4.227.

Karlsrud, K., Jensen, T. G., Wensaas Lied, E. K., Nowacki, F. & Simonsen, A. S. (2014). Significant ageing effects for axially loaded piles in sand and clay verified by new field load tests. *Proceedings of the offshore technology conference, Houston, TX, USA*, paper no. OTC-25197-MS.

Kirwan, L. (2015). *Investigation of ageing mechanisms for axially loaded piles in sand*. PhD thesis, University College Dublin, Dublin, Ireland.

Kuwano, R. & Jardine, R. J. (2002). On measuring creep behaviour in granular materials through triaxial testing. *Can. Geotech. J.* **39**, No. 5, 391–395.

Lehane, B. (1992). *Experimental investigations of pile behaviour using instrumented field piles*. PhD thesis, University of London, Imperial College, London, UK.

Lehane, B., Schneider, J. & Xu, X. (2005). *A review of design methods for offshore driven piles in siliceous sand*, Report no. GEO:05358. Perth, Australia: University of Western Australia.

Lehane, B. M., Schneider, J. A., Lim, J. K. & Mortara, G. (2012). Shaft friction from instrumented displacement piles in an uncemented calcareous sand. *J. Geotech. Geoenviron. Engng* **138**, No. 11, 1357–1368, https://doi.org/10.1061/(ASCE)GT.1943-5606.0000712.

Lehane, B. M., Lim, J. K., Carotenuto, P., Nadim, F., Lacasse, S., Jardine, R. J. & van Dijk, B. (2017). Characteristics of unified database for driven piles. In *Offshore site investigation geotechnics 8th international conference proceeding*, pp. 162–191. London, UK: Society for Underwater Technology.

Lim, J. K. & Lehane, B. M. (2014). Characterisation of the effects of time on the shaft friction of displacement piles in sand. *Géotechnique* **64**, No. 6, 476–485, https://doi.org/10.1680/geot.13.P.220.

Lim, J. K. & Lehane, B. M. (2015). Time effects on the shaft capacity of jacked piles in sand. *Can. Geotech. J.* **52**, No. 11, 1830–1838.

Long, J. H., Kerrigan, J. A. & Wysockey, M. H. (1999). Measured time effects for axial testing of driven piling. *Transp. Res. Board* **1663**, No. 1, 8–15.

Ng, E., Briaud, J. L. & Tucker, L. M. (1988). *Field testing of 5 axially loaded single piles in sand at Hunter's point, research report to FHWA*. San Francisco, CA, USA: Geo Resource Consultants Inc.

NGI (Norwegian Geotechnical Institute) (2014). *Time effects on pile capacity. Summary and evaluation of test results,*

Report 20061251-00-279, Rev. 1 March 2014. Oslo, Norway: NGI.

Schmertmann, J. H. (1991). The mechanical aging of soils. *ASCE J. Geotech. Engng* **117**, No. 9, 1288–1330.

Schneider, J., White, D. & Lehane, B. (2007). Shaft friction of driven piles in siliceous, calcareous and micaceous sands. In *Offshore site investigations and geotechnics: confronting new challenges and sharing knowledge*, pp. 367–382. London, UK: Society of Underwater Technology.

Shek, M. P., Zhang, L. M. & Pang, W. H. (2006). Set-up effect in long piles in weathered soils. *Proc. Instn Civ. Engrs – Geotech. Engng* **159**, No. 3, 145–152, https://doi.org/10.1680/geng.2006.159.3.145.

Skov, R. & Denver, H. (1988). Time-dependence of bearing capacity of piles. In *Proceedings of the 3rd international conference on the application of stress-wave theory to piles* (ed. B. G. Fellenius), pp. 879–888. Ottawa, Canada: BiTech Publishers.

Tavenas, F. & Audy, R. (1972). Limitations of the driving formulas for predicting bearing capacities of driven piles in sand. *Can. Geotech. J.* **9**, No. 1, 47–62.

Tolooiyan, A. & Gavin, K. G. (2013). The base resistance of non-displacement piles in sand, part II – numerical analyses. *Proc. Instn Civ. Engrs – Geotech. Engng* **166**, No. 6, 549–560, https://doi.org/10.1680/geng.11.00100.

Yang, Z. X., Jardine, R. J., Zhu, B. T., Foray, P. & Tsuha, C. H. C. (2010). Sand grain crushing and interface shearing during displacement pile installation in sand. *Géotechnique* **60**, No. 6, 469–482, https://doi.org/10.1680/geot.2010.60.6.469.

York, D. L., Brusey, W. G., Clemente, F. M. & Law, S. K. (1994). Setup and relaxation in glacial sand. *J. Geotech. Engng* **120**, No. 9, 1498–1513.

Zhang, Z. & Wang, Y. H. (2014). Examining setup mechanisms of driven piles in sand using laboratory model pile tests. *J. Geotech. Geoenviron. Engng* **141**, No. 3, 04014114, https://doi.org/10.1061/(ASCE)GT.1943-5606.0001252.

Zhu, B., Jardine, R. J. & Foray, P. (2009). The use of miniature soil stress measuring cells in laboratory applications involving stress reversals. *Soils Found.* **49**, No. 5, 675–688.